On multistabilities of real car's wake

G. Bonnavion[a,*], O. Cadot[a], A. Évrard[a], V. Herbert[b], S. Parpais[c], R. Vigneron[d], J. Délery[d]

[a] *IMSIA, ENSTA-ParisTech, UMR 9219 CNRS, 828 Boulevard des Maréchaux, 91762 Palaiseau Cedex, France*
[b] *PSA Peugeot Citroën, Route de Gisy, 78140 Vélizy-Villacoublay, France*
[c] *Renault SAS, 13/15 Quai Alphonse le Gallo, 92100 Boulogne-Billancourt, France*
[d] *GIE-S2A, 2 Avenue Volta, 78180 Montigny-le-Bretonneux, France*

Abstract

Two different cases of wake transitions are identified with two car models in real flow condition, a hatchback vehicle (Renault Mégane) and a light van (Renault Kangoo). Their wakes are studied thanks to aerodynamic forces and pressure distributions at the car's base. For the hatchback car, a transition yawing angle of $\pm 8.6°$ at which a bistable behavior occurs is identified. It originates from a massive intermittent reattachment occurring simultaneously on the whole slanted rear window. The reattachment is suspected to be caused by the increase in curvature of the separated shear layer as the yaw increases. For the van, reversals of the base pressure distribution are observed for a smaller yawing angle of $\pm 4°$ excluding unambiguously the possibility of a reattachment because of the bluntness of the after-body. A bistable regime between the two reversed states is studied at a yawing angle of $4°$. It is supposed to be caused by a wake instability recently evidenced for the simplified square back Ahmed body that leads to the presence of two distinct static modes of the wake. It is shown that both modes can be permanently selected independently from the bistable configuration.

Keywords: turbulent flow, wake flow, bluff body, cars aerodynamics, wake multistability, wake reversal, bistability, static asymmetric modes, flow reattachment

1. Introduction

Despite the increasing security, comfort and performance requirements of new cars, their fuel consumption has to be kept low enough to satisfy always more stringent pollutants emission standards and has even become a marketing argument. Reducing it drastically has therefore become one of the main short-term goals of the automotive industry. One way to achieve this is to reduce the car's aerodynamic drag. For this reason, the turbulent wake flow behind vehicles is of major interest as the base of a vehicle can generate up to 30% of the total drag and control strategies are currently applied to detached flows.

From the academic point of view, cars are bluff bodies developing a turbulent wake with Reynolds numbers up to few millions. Multistability, if it exists, offers the possibility to the flow to be in different stable states for the exact same conditions. Each stable state corresponds to a turbulent wake having its own global properties about symmetries and mean aerodynamic forces. One of the most spectacular case of multistability occurs during the drag crisis transitions of smooth bluff bodies [1]. In the critical Reynolds number regime of a circular cylinder ($10^5 < \mathrm{Re} < 5\times10^5$), the laminar to turbulent transition of the free boundary layers is accompanied by the occurrence of asymmetric wake flow states [2, 3] producing a non-zero mean lift. They are commonly called one-bubble and two-bubbles transitions and correspond respectively to the reattachment of the free shear turbulent layer on one side and both sides of the cylinder. From global force [4, 5] and local pressure [6] measurements, the existence of bistable behaviors in this critical range has been evidenced through hysteretic discontinuities in the Strouhal - Reynolds numbers relationship. Schewe [4] associates each discontinuity with

*Corresponding author
Email address: bonnavion@ensta.fr (G. Bonnavion)

a subcritical bifurcation during which the energy of the force fluctuations is dominated by the contribution of a wide low frequency domain [4, 5, 6]. Recently, the examination of pressure time series measured on the cylinder [7, 8] revealed that reattachments might switch from one side to the other unpredictably in time during the drag crisis fluctuations. Further analyses [9] confirmed that the strong fluctuations were the consequence of the random exploration of few identified asymmetric and symmetric metastable states of the wake leading to bi- and even to three-stability.

A fundamentally different case of multistability has been recently evidenced in the context of cars aerodynamics [10, 11] with the square back Ahmed body at Reynolds numbers up to few millions. Depending on the base aspect ratio [12], the turbulent wake exhibits a random bistable dynamics either between a top and down or a left and right orientation. The time spent in an orientated state depends crucially on both the yawing and the pitching angles, and a lonely state can easily be permanently selected by geometrical defects. Contrary to the multisability associated with flow reattachment identified as a subcritical bifurcation at large Reynolds numbers, the wake orientation states are identified as a static wake instability resulting from a steady supercritical pitchfork bifurcation in the laminar regime [10], which means that the orientation states are observable in a very wide range of Reynolds number, beginning at the bifurcation point with a critical Reynolds number that can be as low as few hundreds depending on the ground clearance [10, 13] until at least few millions [11, 14]. Since this seeding work, other teams [15, 16] confirmed the existence of two asymmetric modes of the turbulent wake for simplified car models with blunt trailing edge geometry.

The question whether the asymmetric modes of the turbulent wake are observable for real cars has been addressed in [17] by studying unsteady aerodynamics loading of four different car models. The left or right orientation of the wake commonly observed for the square back Ahmed body [10, 11, 13, 14, 15] has never been observed so far but a random bistable dynamic between a top and down orientation of the wake has been found for the Renault Kangoo in [17] for a small yawing angle of 4°. In sideslip conditions, the Ahmed body with a slanted window of 35° also exhibits a bistable dynamics as recently shown in [18] but for yawing angles larger than 10°. This last finding indicates that bistability phenomena are not only associated with blunt after body geometry but could be extended to real cars having slanted rear windows.

The aim of this paper is to elucidate the origin of bistability depending on the afterbody shape and whether it is induced by turbulent reattachment phenomena or a global wake instability. We will address this issue with two car series models in real flow condition. The Renault Kangoo has been chosen because its afterbody is comparable to the square back Ahmed geometry and the Renault Mégane that is comparable to the 35° slanted window Ahmed body [19].

The paper is organized as follows. Section 2 describes the scale 1 wind tunnel, the two car models and the measurements of both the aerodynamic forces and pressure. Results are presented in five parts in section 3. Section 3.1 characterizes the references cases of both vehicles when they are aligned with the incoming flow. The influence of the yawing angle is first studied in a wide range of sideslip conditions in section 3.2, then the two following sections focus on the critical yawing angle of multistability for the Renault Mégane in section 3.3 and Renault Kangoo in section 3.4. The last part of the results, section 3.5, is devoted to the selection of the wake states of the Kangoo. Results are discussed in section 4 with the aim to shed light on two possible mechanisms responsible for the observed bistable behaviors and their consequences on the wake and on the aerodynamic forces respectively in sections 4.1 and 4.2. Section 5 concludes the work.

2. Experiments

2.1. Wind tunnel and models

The experiments are carried out in the full-scale wind tunnel of the GIE-S2A in Montigny-le-Bretonneux (France)[1], fully described in Waudby-Smith *et al.* [20]. In this wind-tunnel, the road effect is simulated by a 6 m-long and 1 m-wide rolling belt located below the vehicle and the four vehicle's wheels are rotating. The plenum is 22.7 m long, 14.0 m wide and 10.4 m high and the test section of 24 m^2 is a 3/4 open jet. The turbulence rate of the facility is 0.4%. A schematic is shown in Fig. 1 where the green rectangle stands for the moving belt.

[1] Souffleries Aéroacoustiques Automobiles: `http://www.soufflerie2a.com/en/`

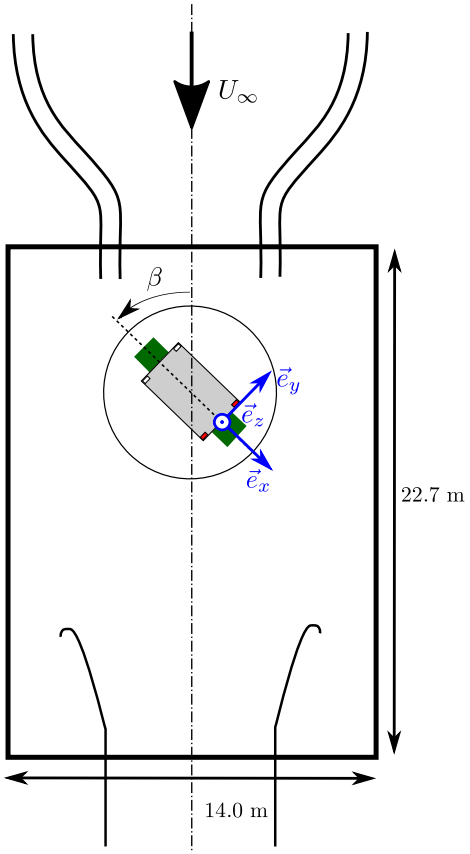

Figure 1: Schematic view of the test section and definition of yawing angle β and of the coordinate system $(\vec{e_x}, \vec{e_y}, \vec{e_z})$ associated with the car.

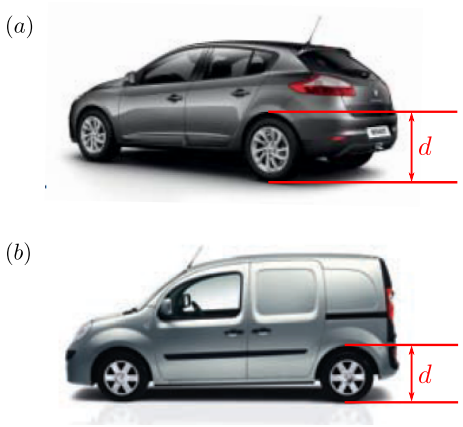

Figure 2: Side view of cars and definition of d: (a) Renault Mégane - (b) Renault Kangoo

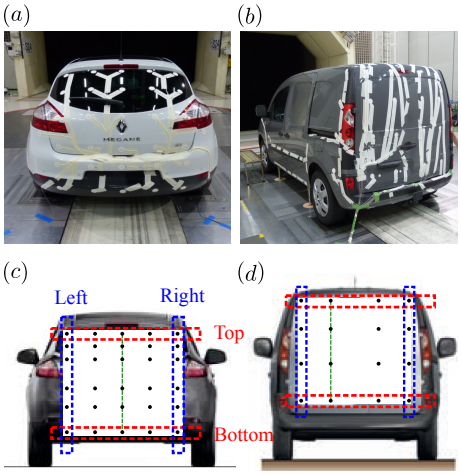

Figure 3: Cars equipped with pressure taps in the GIE S2A full-scale wind tunnel (a, b) and location of pressure taps (c, d): (a, c) Renault Mégane - (b, d) Renault Kangoo. The top and bottom (resp. left and right) lines are used to compute the vertical (resp. horizontal) base pressure gradient as defined in Eq. (5)–(6). The green vertical lines $y^* = 0$ for the Mégane and $y^* = -0.16$ for the Kangoo are used for space-time diagrams (Fig. 13 and Fig 19).

Two different car models are tested: a Renault Mégane III and a Renault Kangoo II shown in Fig. 2. While the first one is a hatchback vehicle with a rounded rear geometry, the other one is a light van with sharp edges and a vertical base. The vehicle's base dimensions are given in Tab. 1 together with the distances d_{front} and d_{rear} defined in Fig. 2 between the top of the wheel arch and the ground for each axis.

The yaw of the vehicle can be precisely adjusted owing to a rotating table whose precision lies below 0.1°. The yawing angle β is defined in Fig. 1 and $\beta = 0.0°$ corresponds to the vehicle aligned with the incoming flow. The range $\beta \in [-10.0°; 10.0°]$ is considered for the Renault Mégane, $\beta \in [-8.0°; 8.0°]$ for the Renault Kangoo. In each of these ranges, clear transitions in the wake have been observed whose investigations bring the contribution of the paper. The freestream velocity is set to $U_\infty = 38.9$ m.s^{-1} ($U_\infty = 140$ km.h^{-1}) for the Mégane and to $U_\infty = 33.3$ m.s^{-1} ($U_\infty = 120$ km.h^{-1}) for the Kangoo. The corresponding Reynolds numbers calculated with the heights of the bases of the vehicles are $\mathrm{Re}_H^{Megane} = 2.5 \times 10^6$ and $\mathrm{Re}_H^{Kangoo} = 3.14 \times 10^6$ respectively.

All non-dimensionalizations are performed using the vehicle's base height H, the freestream velocity

Table 1: Geometrical characteristics of the vehicles.

Parameter	Mégane	Kangoo [17]
Base height H (m)	1.000	1.480
Base width W (m)	1.810	1.650
Aspect ratio $W^* = W/H$	1.810	1.115
Frontal surface S (m^2)	2.210	2.840
d_{front} (m)	0.667	0.722
d_{rear} (m)	0.671	0.687

of the incoming flow U_∞ and the fluid's density ρ and are denoted by *. Therefore, the dimensionless time is obtained by dividing by the convective time scale H/U_∞: $t^* = (U_\infty t)/H$.

2.2. Measurements of the aerodynamic forces and pressure

The six-components aerodynamic balance of the facility, provided by Schenck GmbH, records the aerodynamic forces at a sampling frequency of 10 Hz during test campaigns. Its uncertainty lies below 2 N for all forces [20]. The drag f_d, the side force f_s and the lift f_l are respectively the components of the aerodynamic load in the coordinate system $(\vec{e}_x, \vec{e}_y, \vec{e}_z)$ defined in Fig. 1 and used throughout. The associated aerodynamic coefficients are defined in Eq. (1), where S is the vehicle's frontal surface given in Tab. 1, U_∞ the freestream velocity and ρ the fluid's density. According to the precision of the balance, the uncertainties on these coefficients are of the order of 10^{-3}.

$$\begin{aligned} Sc_d(t^*) &= \frac{f_d(t^*)}{\frac{1}{2}\rho U_\infty^2} \\ Sc_s(t^*) &= \frac{f_s(t^*)}{\frac{1}{2}\rho U_\infty^2} \\ Sc_l(t^*) &= \frac{f_l(t^*)}{\frac{1}{2}\rho U_\infty^2} \end{aligned} \tag{1}$$

Both vehicles are equipped with pressure taps placed almost uniformly on the base at the locations (y^*, z^*) shown in Fig. 3(c) and Fig. 3(d). 30 taps are used for the Mégane and 16 for the Kangoo. Measurements of the pressure p are made thanks to a pressure scanner from Mescan (ZOC22 for the Mégane, ZOC33 for the Kangoo). The sampling frequency is set to 200 Hz for the Mégane and $2-3$ Hz for the Kangoo and the precision is of the order of ± 3.75 Pa. The results are not affected by the difference in the sampling frequency as the phenomena discussed in this paper are at least two order of magnitude slower than the acquisition.

The coefficient of pressure c_p is computed as:

$$c_p(y^*, z^*, t^*) = \frac{p(y^*, z^*, t^*) - p_\infty}{\frac{1}{2}\rho U_\infty^2} \tag{2}$$

where the freestream pressure p_∞ measured upstream is used as the reference. Pressure distributions $C_p(y^*, z^*)$ are used to display the mean pressure distribution at the base using a cubic interpolation.

A first global quantity of interest is the base suction coefficient C_b defined as:

$$C_b = -\frac{1}{N}\sum_{i=1}^{N} C_p(y_i^*, z_i^*) \tag{3}$$

where N is the number of pressure taps at the base and (y_i^*, z_i^*) the dimensionless location of the i-th tap. By definition, the base suction coefficient C_b is positive and has to be minimized in order to reduce the drag generated at the base. According to the accuracy of pressure measurement, the uncertainties on c_p and thus on C_b are of the order of 2×10^{-3}.

Other quantities of interest are the vertical and horizontal base pressure gradients. They are computed from the pressure taps located at the contour of the vehicle's base as indicated in Fig. 3(c) and Fig. 3(d) and spatially averaged as follows:

$$\begin{aligned} c_{p_{top}}(t^*) &= \frac{1}{n_c}\sum_{i=1}^{n_c} c_p(y_i^*, z_{i,top}^*, t^*) \\ c_{p_{bottom}}(t^*) &= \frac{1}{n_c}\sum_{i=1}^{n_c} c_p(y_i^*, z_{i,bottom}^*, t^*) \\ c_{p_{left}}(t^*) &= \frac{1}{n_r}\sum_{i=1}^{n_r} c_p(y_{i,left}^*, z_i^*, t^*) \\ c_{p_{right}}(t^*) &= \frac{1}{n_r}\sum_{i=1}^{n_r} c_p(y_{i,right}^*, z_i^*, t^*) \end{aligned} \tag{4}$$

where n_r stands for the number of rows and n_c the number of columns. The *bottom* pressure coefficient given in Eq. (4) is substracted from the *top* one and then divided by the distance δ_z between the top and the bottom rows to give a vertical base pressure gradient denoted $\frac{\partial c_p}{\partial z}$, itself non-dimensionalized by H:

$$\frac{\partial c_p}{\partial z^*}(t^*) = H\frac{c_{p_{top}}(t^*) - c_{p_{bottom}}(t^*)}{\delta_z} \tag{5}$$

Similarly, the horizontal base pressure gradient $\frac{\partial c_p}{\partial y^*}$ is:

$$\frac{\partial c_p}{\partial y^*}(t^*) = H \frac{c_{p_{right}}(t^*) - c_{p_{left}}(t^*)}{\delta_y} \qquad (6)$$

For each yawing angle considered, the aerodynamic forces and the base pressure are recorded for 2 to 6 minutes. From these data, time series $a(t)$ of force coefficients or base pressure gradients are analyzed with statistical tools such as temporal mean $A = \overline{a}$ and Probability Density Functions PDF(a). Fluctuations of the quantities correspond to the standard deviation denoted by $a' = \sqrt{\overline{(a-A)^2}}$.

3. Results

The results for the reference case for the vehicles aligned with the flow are presented in section 3.1. A parametric study of the yawing angle β is then made for both cars in section 3.2. Two identified characteristic angles are studied in sections 3.3 for the Mégane and 3.4 for the Kangoo. Finally, section 3.5 focuses on the selection of wake topology behind the Renault Kangoo.

3.1. Reference case: Vehicles aligned with the incoming flow ($\beta = 0.0°$)

The mean base pressure distributions $C_p(y^*, z^*)$ for the Renault Mégane and the Renault Kangoo when aligned with the flow are given respectively in Fig. 4(a) and Fig. 4(b). The Mégane shows a very uniform pressure distribution at the base almost symmetric in the y-direction and with a very small vertical gradient, while a significant positive vertical pressure gradient exists for the Kangoo. The probability density functions of the base pressure gradients $\frac{\partial c_p}{\partial y^*}$ and $\frac{\partial c_p}{\partial z^*}$ defined in Eq. (5) and (6) are plotted in Fig. 4(c) and Fig. 4(d) for the Mégane and the Kangoo respectively. They both display a single peak that defines without ambiguity a single mean flow state. Fluctuations around the mean are larger for the Kangoo than for the Mégane.

The values of the mean aerodynamic coefficients and base pressure gradients are given for the reference case in Tab. 2. The mean vertical base pressure gradient on the Kangoo is positive and equal to 0.152, which seems surprising according to the significantly positive lift: a lower pressure would indeed have been expected at the top of the base rather than at its bottom. For the Mégane though, the vertical base pressure gradient is almost zero.

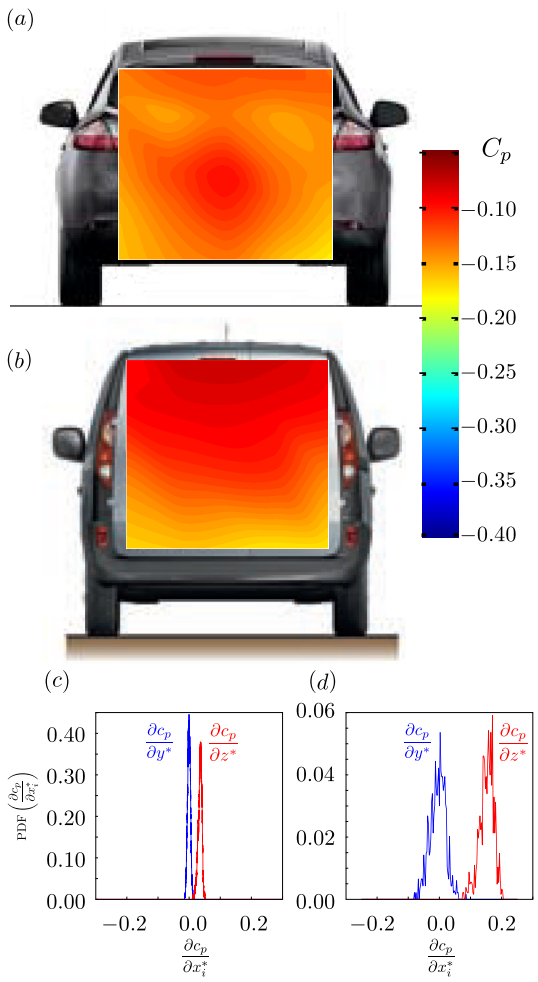

Figure 4: Mean base pressure distribution $C_p(y^*, z^*)$ at $\beta = 0.0°$: (a) Renault Mégane - (b) Renault Kangoo. Probability density functions of $\frac{\partial c_p}{\partial y^*}$ (in blue) and $\frac{\partial c_p}{\partial z^*}$ (in red): (c) Renault Mégane - (d) Renault Kangoo

The behavior of global quantities (aerodynamic coefficients and base pressure gradients) with respect to yaw is studied in section 3.2.

3.2. Influence of the yawing angle

The mean force coefficients SC_d, SC_s and SC_l and mean base pressure gradients $\frac{\partial C_p}{dy^*}$ and $\frac{\partial C_p}{dz^*}$ are given in Fig. 5 and in Fig. 6 as a function of the yawing angle β. The coefficient associated with the lateral force (SC_s) shows a linear evolution with respect to yaw for both cars. As concerns the Mégane, a sudden increase of the lift coefficient SC_l can be observed for yawing angles larger in absolute value

Table 2: Mean values of global parameters in the reference case with $\beta = 0.0°$

Parameter	Renault Mégane	Renault Kangoo
SC_d (m^2)	0.744	0.986
SC_s (m^2)	-0.005	0.016
SC_l (m^2)	0.218	0.231
C_d	0.336	0.351
$\frac{\partial C_p}{\partial y^*}$	$< 10^{-3}$	-0.005
$\frac{\partial C_p}{\partial z^*}$	0.035	0.152

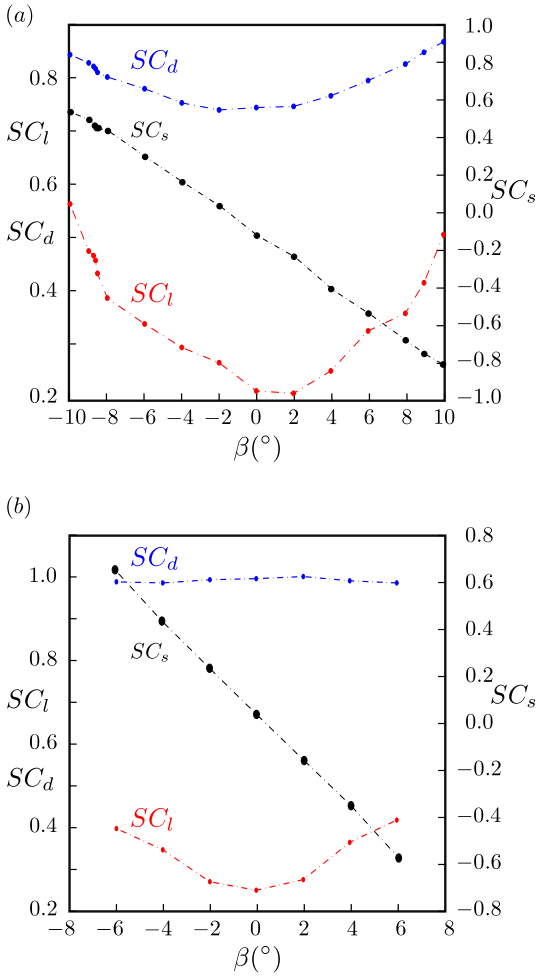

Figure 5: Evolution of SC_d (blue), SC_s (black) and SC_l (red) as a function of the yawing angle β: (a) Renault Mégane - (b) Renault Kangoo

than $|\beta| = 8.0°$. Similarly, the drag increases faster in these ranges. For the Kangoo, it is noticeable that the drag coefficient SC_d is almost constant in spite of the increase of yaw. The lift coefficient SC_l shows a quicker increase for angles such that $|\beta| \approx 4.0°$. Also, as expected due to the apparent symmetry of cars, all coefficients but SC_s are roughly even functions of the yawing angle β for both vehicles. However, some discrepancies are observable in Fig. 5 as for SC_l at $\beta = 2.0°$ for the Mégane and for SC_s that is not exactly equal to zero for both cars when aligned with the incoming flow at $\beta = 0.0°$. These symmetry defects are not related to measurements uncertainties but to the flow produced by the asymmetrical parts of the vehicles such as the air intake duct or underbody details.

In order to have a better understanding of the origin of these variations, mean values of the base pressure gradients are plotted as a function of the yawing angle in Fig. 6. The horizontal base pressure gradients do not show any significant dependence on yaw and are much smaller than the corresponding vertical base pressure gradients. An anomaly showing high sensitivity to β exists for the vertical base pressure gradients of both cars: for the Renault Mégane, it changes from almost zero to a negative value as the absolute value of yawing angle reaches $|\beta| = 8.0°$; for the Kangoo, from a positive value to almost zero as $|\beta| = 4.0°$. This substantial evolution is correlated with the lift increase (drag as well for the Mégane) as the angles detected here are the same than those found before (Fig. 5 and Fig. 6).

The fluctuations are now studied in Fig. 7 and in Fig. 8 respectively. For the Mégane, it is clear that transitions around $|\beta| = 8.0°$ are associated with large fluctuations of the lift shown in Fig. 7(a) and of the vertical base pressure gradient in Fig. 8(a). Similarly, the sudden decrease in vertical base pressure gradient of the Kangoo at $|\beta| = 4.0°$ is associated with a large increase in fluctuations of both the lift (Fig. 7b) and the vertical base pressure gradient (Fig. 8b). The angles corresponding to the maximum fluctuations of the lift will define critical angles: $\beta = \pm 8.6°$ and $\beta = \pm 4.0°$ for the Mégane and the Kangoo respectively. The transitions of the wake discussed below occur for negative and positive values of the yawing angle for both cars. Nevertheless, wake bi-stability studied in section 3.4 for the Renault Kangoo only occurs at the positive value $\beta = 4.0°$ [17] without further impacts on the transition.

The wake properties around the critical angles

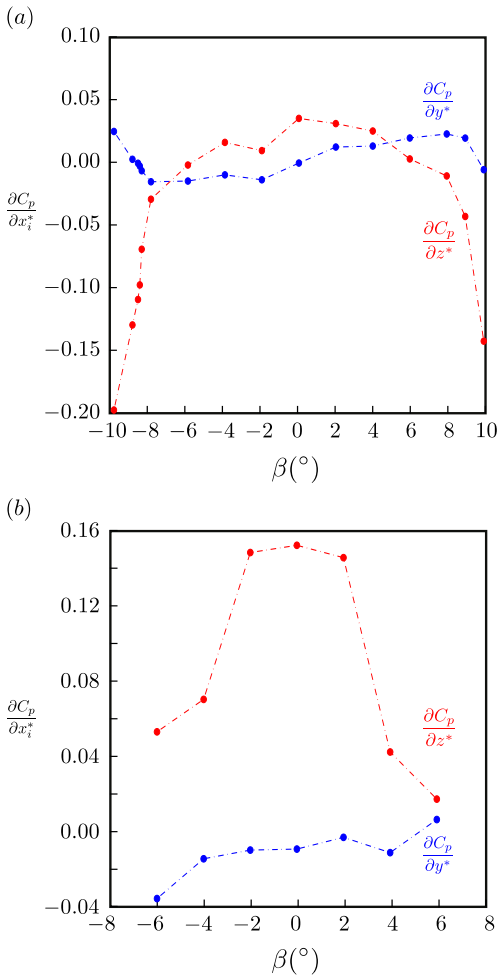

Figure 6: Evolution of $\frac{\partial C_p}{\partial y^*}$ (blue) and $\frac{\partial C_p}{\partial z^*}$ (red) as a function of the yawing angle β: (a) Renault Mégane - (b) Renault Kangoo

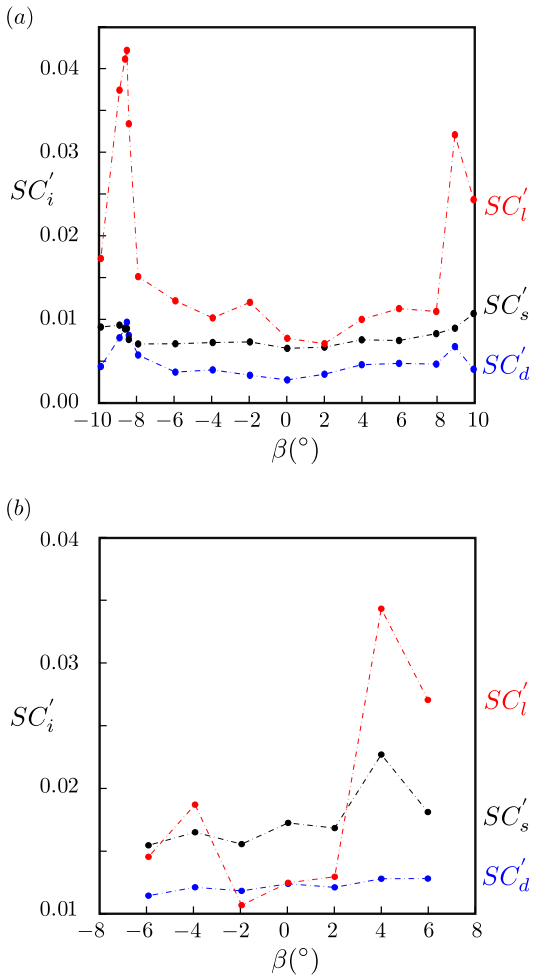

Figure 7: Evolution of SC_d' (blue), SC_s' (black) and SC_l' (red) as a function of the yawing angle β: (a) Renault Mégane - (b) Renault Kangoo

can be identified on account of the mean base pressure distributions $C_p(y^*, z^*)$ for both vehicles (Fig. 9 and Fig. 10). The large low-pressure area that appears on the whole rear window of the Mégane at $\beta = -10.0°$ is caused by a massive boundary layer reattachment whose dynamics is characterized in details in section 3.3. It is interesting to notice that, in spite of the increase of the yawing angle, the left-right symmetry of the base pressure distribution is almost preserved.

For the Kangoo, the area of high pressure disappears at the critical angle and the base pressure distribution becomes more uniform leading the vertical base pressure gradient down to almost zero. Unlike the Mégane, this change cannot be related to massive flow reattachment because the blunt after-body geometry does not allow it for such a small yawing angle. It corresponds more likely to a wake reversal due to a wake instability as clarified in section 3.4.

3.3. Wake multistability for the Renault Mégane

Time series of the lift coefficient of the Mégane are plotted in Fig. 11. Three distinct yawing angles around the critical value are considered: $\beta = -8.0°$, $\beta = -10.0°$ and the critical angle $\beta = -8.6°$. As $\beta = -8.6°$, the lift seems to have bounded and random fluctuations. The lower limit is close to the mean value for $\beta = -8.0°$ and the upper to that for $\beta = -10.0°$.

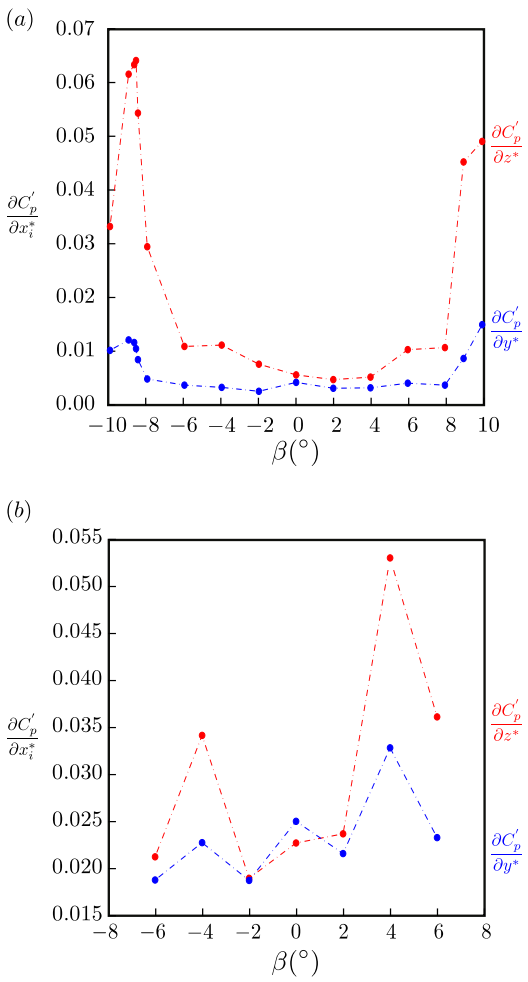

Figure 8: Evolution of $\frac{\partial C_p}{\partial y^*}'$ (blue) and $\frac{\partial C_p}{\partial z^*}'$ (red) as a function of the yawing angle β: (a) Renault Mégane - (b) Renault Kangoo

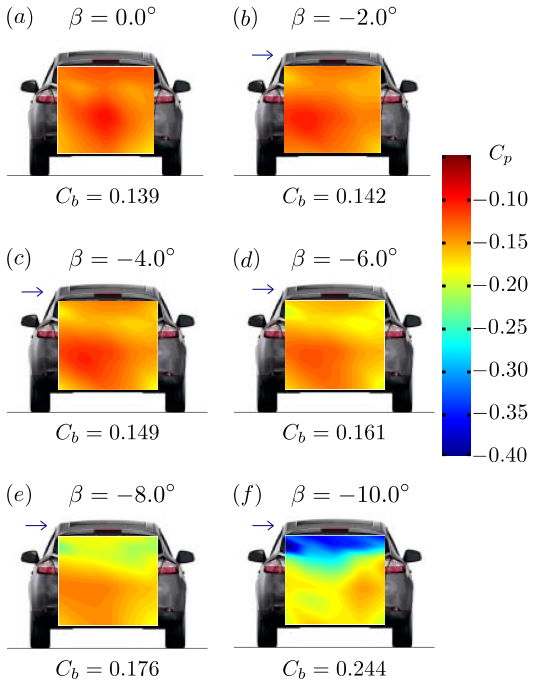

Figure 9: Mean base pressure distribution $C_p(y^*, z^*)$ for the Renault Mégane: (a) $\beta = 0.0^\circ$ - (b) $\beta = -2.0^\circ$ - (c) $\beta = -4.0^\circ$ - (d) $\beta = -6.0^\circ$ - (e) $\beta = -8.0^\circ$ - (f) $\beta = -10.0^\circ$. The horizontal arrow stands for the lateral component of the velocity $U_\infty \sin(\beta)$ (not to scale).

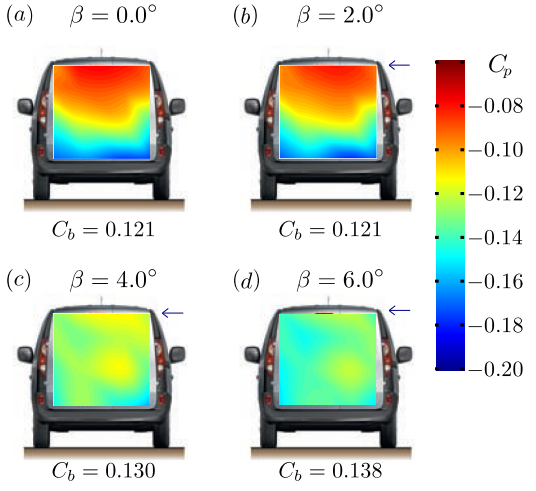

Figure 10: Mean base pressure distribution $C_p(y^*, z^*)$ for the Renault Kangoo: (a) $\beta = 0.0^\circ$ - (b) $\beta = 2.0^\circ$ - (c) $\beta = 4.0^\circ$ - (d) $\beta = 6.0^\circ$. The horizontal arrow stands for the lateral component of the velocity $U_\infty \sin(\beta)$ (not to scale).

The existence of two preferred values of the lift is confirmed by the two peaks of the probability density function shown in Fig. 12. These two peaks are indistinguishable for the drag because of the large turbulent fluctuations.

The temporal evolution of the base pressure distribution is a good indicator of the wake dynamics. The space-time diagram in Fig. 13 shows the pressure coefficient along the vertical line $y^* = 0$. A low-pressure area intermittently appears and disappears on the vehicle's rear window. The characteristic time of this process is about $1,000$ times longer than the convective time H/U_∞. No periodicity is associated with this phenomenon as indicated by the absence of peaks in the spectral power density of the vertical base pressure gradient given in Fig. 14. Compared to the sub-critical case $\beta = -8.0^\circ$ and to the super-critical case $\beta = -10.0^\circ$, a large range

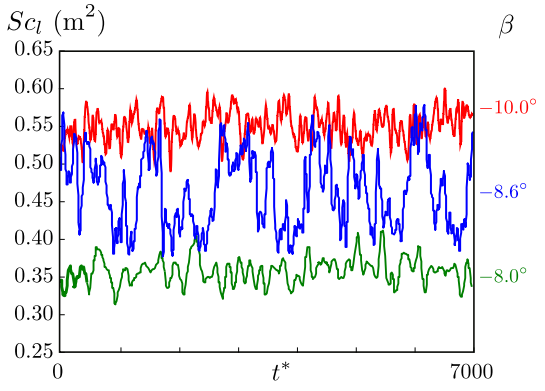

Figure 11: Time series of the lift coefficient Sc_l for the Renault Mégane at different yawing angles: *Red*: $\beta = -10.0°$ - *Blue*: $\beta = -8.6°$ - *Green*: $\beta = -8.0°$

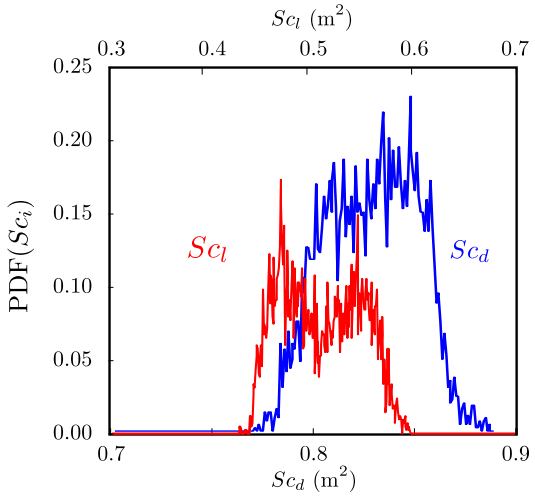

Figure 12: Probability density functions of Sc_d (in blue) and Sc_l (in red) for the Renault Mégane ($\beta = -8.6°$)

of low frequencies is impacted which corresponds to random events.

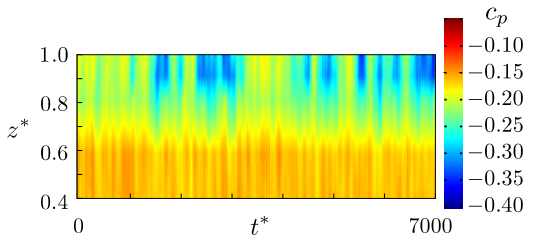

Figure 13: Space-time diagram of $c_p(y^* = 0, z^*, t^*)$ along the line $y^* = 0$ shown in Fig. 3(c) for Renault Mégane at $\beta = -8.6°$

The probability density function of the vertical

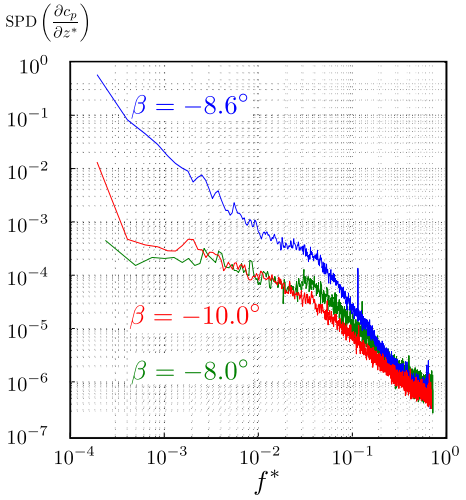

Figure 14: Spectra of $\frac{\partial c_p}{\partial z^*}$ for the Renault Mégane: *(green)* Sub-critical case $\beta = -8.0°$ - *(blue)* Critical case $\beta = -8.6°$ - *(red)* Super-critical case $\beta = -10.0°$

base pressure gradient at the critical angle is presented in Fig. 15. As for the lift coefficient in Fig. 12, two preferred values of the gradient are identified by the presence of two peaks. The natural separation between the two associated states is shown in this plot: values of $\frac{\partial c_p}{\partial z^*}$ above -0.1 belong to *state D* while values below to *state A*. As discussed later in section 4.1, A stands for attached and D for detached shear layer. Conditional averaging is performed using this criterion to obtain the corresponding base pressure distributions in Fig. 16(a) and Fig. 16(b). For comparison, base pressure distributions for sub- and super-critical yawing angles are also given in Fig. 16(c) and Fig. 16(d). *State D* appears to be closer to the sub-critical configuration while *state A* is much more similar to the super-critical topology. The multistable state is consequently a transition between these limits.

Only negative values of the yawing angle are discussed in this section. Nevertheless, due to the general symmetry of the car with respect to the z-axis, similar results are obtained for positive yawing angles as the force coefficients and mean base pressure gradient follow a roughly even behavior with respect to the yaw (Fig. 5a, 6a, 7a and 8a).

To summarize, a bistable behavior is observed for the Mégane during the transition between the flow being massively detached from the base (sub-critical configuration D for $|\beta| \leq 8.0°$) and the global reattachment on the rear window (super-

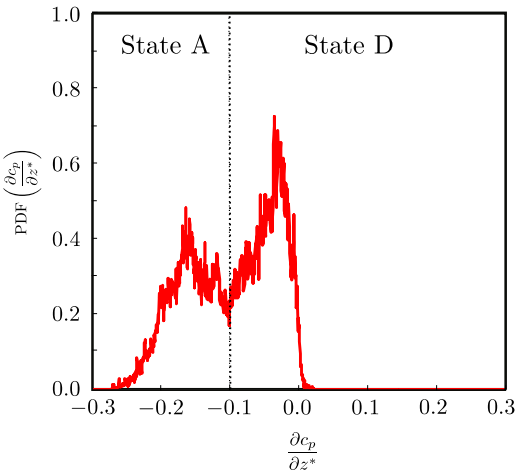

Figure 15: Probability density function of $\frac{\partial c_p}{\partial z^*}$ (Renault Mégane, $\beta = -8.6°$) and definition of *state A* and *state D*.

critical configuration A for $|\beta| \geq 10.0°$).

3.4. Wake multistability for the Renault Kangoo

We now focus on the transition occurring at $\beta = 4.0°$ for the Kangoo. Time series of the lift coefficient are plotted for $\beta = 2.0°$, $\beta = 4.0°$ and $\beta = 6.0°$ in Fig. 17. The lift fluctuates following a random process in the case $\beta = 4.0°$ bounded by the values at $\beta = 2.0°$ and $\beta = 6.0°$. The bimodal probability density function given in Fig. 18 indicates two preferred values of the lift as already shown by Cadot *et al.* [17].

A space-time diagram of the pressure distribution along the vertical line $y^* = -0.16$ is plotted in Fig. 19. We can observe that the location of the lowest pressure switches randomly from the bottom to the top of the base thus changing the sign of the vertical gradient. This corresponds to wake reversals. The characteristic time of these reversals corresponds to a long-time dynamics of about 250 convective times. As for the Mégane, these fluctuations correspond to a random low-frequency phenomenon as can be seen in Fig. 20. It is characterized by a huge increase of energy at low frequencies compared to the non-fluctuating cases.

The bimodal probability density function of $\frac{\partial c_p}{\partial z^*}$ associated with $\beta = 4.0°$ is given in Fig. 21. The two preferred states are defined as follows: values of $\frac{\partial c_p}{\partial z^*}$ above 0.04 belong to *state T* and values below to *state B*. The wake is consequently oriented either towards the top of the base either towards its bottom. The first case is referred as *state T*, the second

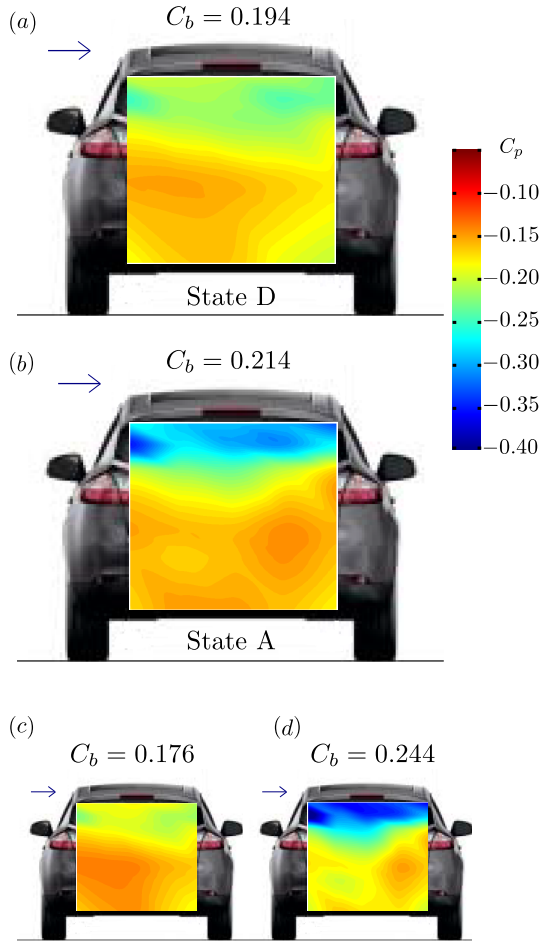

Figure 16: Mean base pressure distribution $C_p(y, z)$ for the Renault Mégane under different configurations: (*a*) *State D* of the multistable configuration ($\beta = -8.6°$) - (*b*) *State A* of the multistable configuration ($\beta = -8.6°$) - (*c*) In the sub-critical range ($\beta = -8.0°$) - (*d*) In the super-critical range ($\beta = -10.0°$)

as *state B*. The mean base pressure distributions $C_p(y^*, z^*)$ corresponding to each state obtained by conditional averaging are given in Fig. 22.

In short, a bistable behavior is observed for the Kangoo at $\beta = 4.0°$. It does not correspond to flow reattachment but to top-bottom wake reversals. Selection of the associated pressure distributions is performed in section 3.5.

3.5. Wake selection behind the Renault Kangoo

Blocking the air-intake as shown in Fig. 23 or changing the pitching angle of the car leads to wake selection.

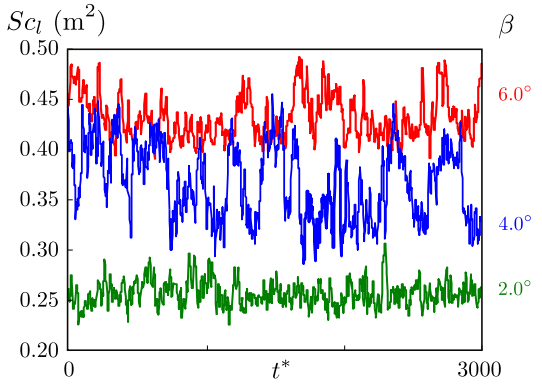

Figure 17: Time series of lift coefficient Sc_l for the Renault Kangoo for: $\beta = 2.0°$ (green), $\beta = 4.0°$ (blue), $\beta = 6.0°$ (red)

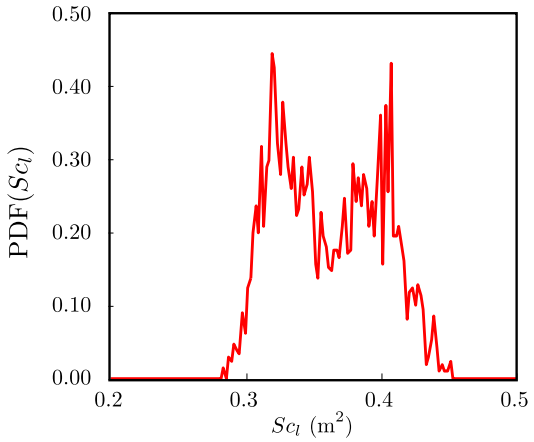

Figure 18: Probability density function of Sc_l for the Renault Kangoo ($\beta = 4.0°$)

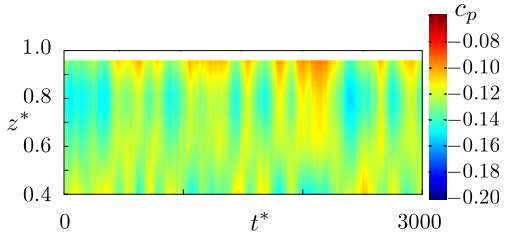

Figure 19: Space-time diagram of $c_p(y^* = -0.16, z^*, t^*)$ along the line $y^* = -0.16$ shown in Fig. 3(d) for the Renault Kangoo at $\beta = +4.0°$

From the bistable case at $\beta = 4.0°$, adding 35 mm to d_{rear} selects the *state* T with the positive base pressure gradient. The obtained base pressure distribution in Fig. 24(a) is quasi-identical to *state* T in Fig. 22(a) observed during bistability. The single peak of the probability density function in

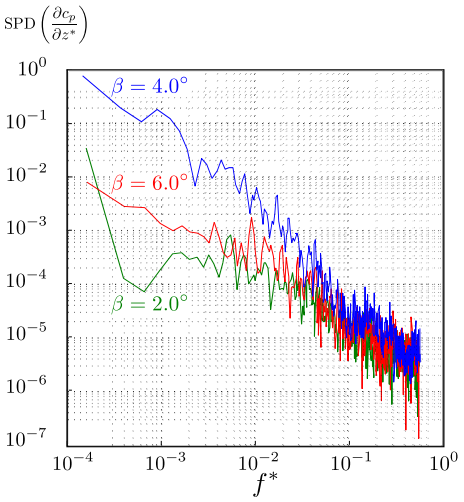

Figure 20: Spectra of $\frac{\partial c_p}{\partial z^*}$ for the Renault Kangoo: *(green)* $\beta = 2.0°$ - *(blue)* Multistable case $\beta = 4.0°$ - *(red)* $\beta = 6.0°$

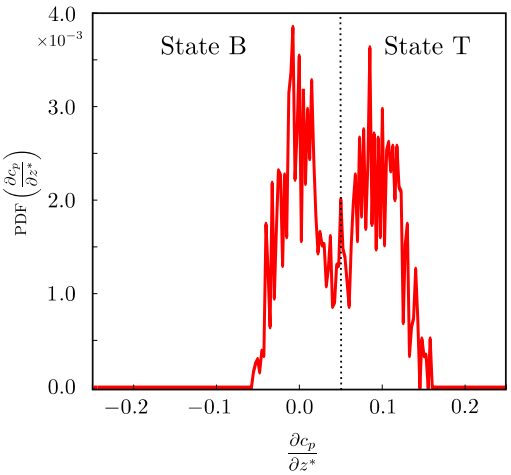

Figure 21: Probability density function of $\frac{\partial c_p}{\partial z^*}$ for the Renault Kangoo ($\beta = +4.0°$) and definition of *state* T and *state* B

Fig. 24(b) ensures that the state with the positive base pressure gradient is mostly present.

The *state* B of the bistable regime shown in Fig. 22(b) can be selected by blocking the air-intake. The base pressure distribution in Fig. 24(c) also has a negative vertical base pressure gradient and the single peak in Fig. 24(d) ensures that this state is stable.

Mode selection can also be performed when the Kangoo is aligned with the flow (*i.e.* $\beta = 0.0°$), in a case where bistability is not present. The natural case exhibits a positive vertical base pressure

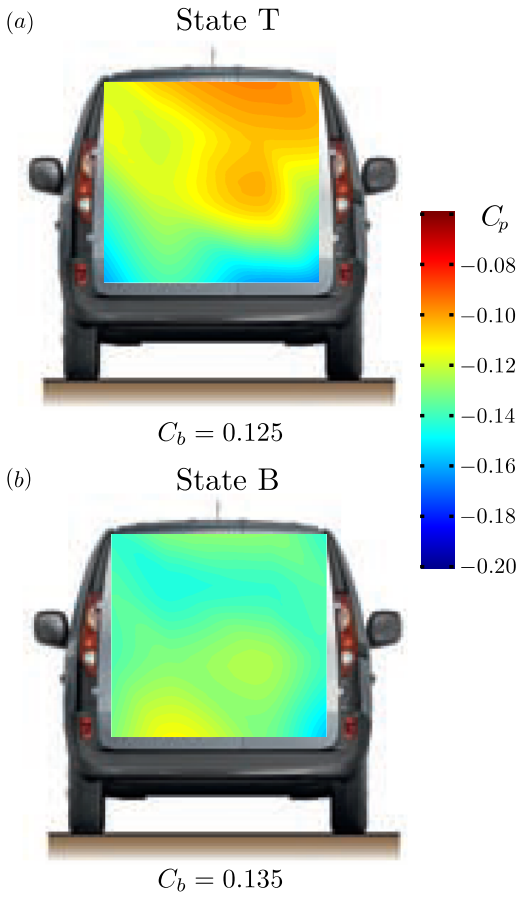

Figure 22: Conditionally averaged base pressure distribution $C_p(y^*, z^*)$ for the Renault Kangoo ($\beta = +4.0°$): (*a*) *State T* - (*b*) *State B*

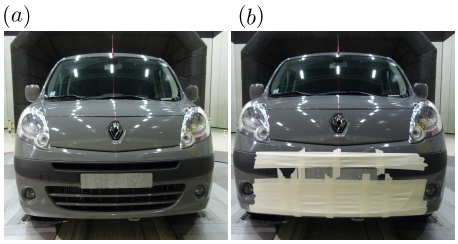

Figure 23: Renault Kangoo: (*a*) Open air-intake - (*b*) Closed air-intake

gradient. The base pressure distribution and the single-peak probability density function are given in Fig. 24($e - f$). Blocking the air-intake leads to a negative vertical pressure gradient indicating wake reversal from top to bottom as depicted in Fig. 24($g - h$).

4. Discussion

Two different causes of wake multistability have been identified in sections 3.3 for the Renault Mégane and 3.4 for the Renault Kangoo. They have been associated with two different physical phenomenon as detailed in these sections. The discussion first focuses on the differences between flow reattachment and wake instability in section 4.1 and section 4.2 details the consequences on the aerodynamic forces.

4.1. Turbulent flow reattachment versus wake instability

As regards the Mégane, the wake bistability observed for $\beta = -8.6°$ in section 3.3 corresponds to flow reattachment. The left-right symmetry of the base pressure distribution is conserved even at high yawing angles which, added to the fact that reattachment occurs on the whole rear window as shown in Fig. 9(f), suggests that an explanation can be found at the car's scale. The base suction coefficient C_b increases continuously with the yawing angle in the detached configuration shown in Fig. 9($a - e$) which corresponds to a pressure decrease at the car's base. Based on the classical potential approach of inviscid detached flows [21], lower base pressure indicates larger curvature of the recirculation zone of the car. Since the separation point is fixed by the spoiler, a larger curvature of the dividing streamline (emanating from the separation point) of the mean flow implies that the shear layer is in average closer to the slanted rear window. Besides, curvature increase with growing yawing angle is also consistent with the pressure drop on the vehicle's roof attested by the increase of the lift force highlighted in Fig. 5(a) together with the decrease of the vertical base pressure gradient $\frac{\partial C_p}{\partial z^*}$ shown in Fig. 6(a). The critical angle corresponds to the situation when the shear layer is close enough from the vehicle to trigger reattachment similarly to the drag crisis in simple geometries [1]. Furthermore, as the pressure is almost uniform on the rear window in the subcritical regime, the flow reattaches simultaneously over the whole width of the vehicle. This mechanism should explain the wake multistability observed for an Ahmed body with a 35°-slant angle by Meile *et al.* [18]. Their critical angle of $\beta = 12.5°$ is, as the one of the Mégane, much larger than the critical value associated with wake multistability caused by static asymmetric modes as in the case of the Kangoo. Moreover, both the lift and

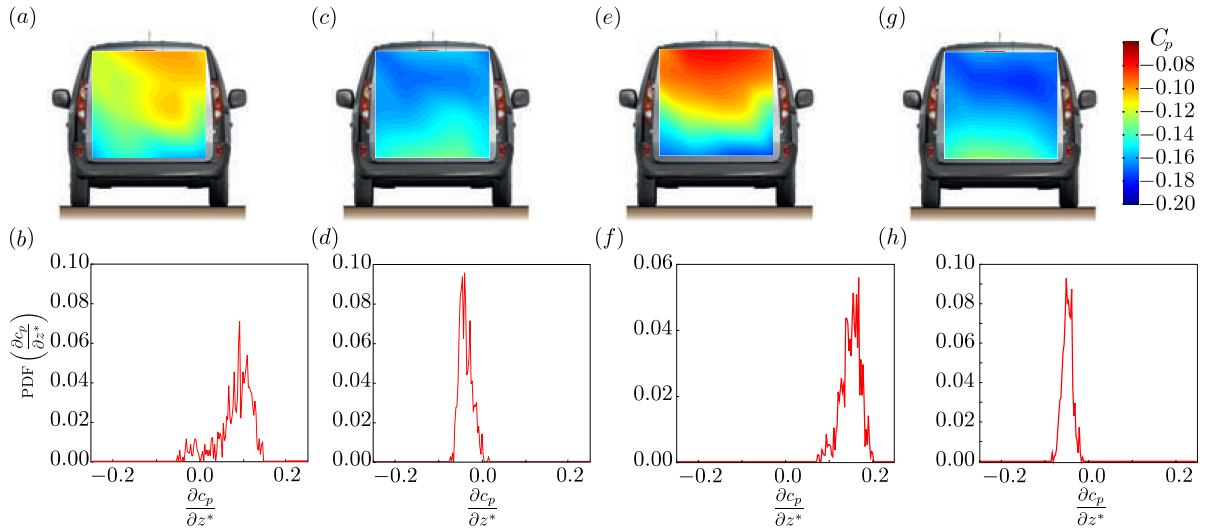

Figure 24: Renault Kangoo with $d_{rear} = 0.722$ m. *Mode T* selected at $\beta = +4.0°$: (a) Mean base pressure distribution $C_p(y^*, z^*)$ - (b) Associated probability density function of $\frac{\partial c_p}{\partial z^*}$; *mode B* selected at $\beta = +4.0°$ with closed air-intake: (c) Mean base pressure distribution $C_p(y^*, z^*)$ - (d) Associated probability density function of $\frac{\partial c_p}{\partial z^*}$; ; *mode T* selected at $\beta = 0.0°$: (e) Mean base pressure distribution $C_p(y^*, z^*)$ - (f) Associated probability density function of $\frac{\partial c_p}{\partial z^*}$; ; *mode B* selected at $\beta = 0.0°$ with closed air-intake: (g) Mean base pressure distribution $C_p(y^*, z^*)$ - (h) Associated probability density function of $\frac{\partial c_p}{\partial z^*}$.

the drag around the critical angle have very similar behaviors to those highlighted in the present work. From the flow visualizations provided, flow reattachment also occurs on the whole width of the body. The detached and attached flow configurations have already been identified by Hucho [22] and called respectively the fastback and the squareback flow regimes but, to our knowledge, this kind of wake bistability on real vehicles has never been reported so far.

As regards the Kangoo, flow reattachment cannot happen because of the geometry of the rear part of the van. This argument is sufficient to reject wake bistability caused by turbulent reattachment as for the Mégane. A reasonable explanation is the presence of static asymmetric modes due to a wake instability [10]. A wake reversal is observed in section 3.4 and characterized by an inversion of the vertical base pressure gradient from one flow configuration to another. The associated base pressure distributions in Fig. 22 let clearly appear that the low pressure area moves from the top to the bottom of the base. The two states identified during the bistability using conditional averaging in Fig. 22 can be retrieved at any yawing angle as for instance at $\beta = 4.0°$ in Fig. 24($a - b - c - d$) or at $\beta = 0.0°$ in Fig. 24($e - f - g - h$). This accounts for the existence of two solutions for the wake that exist after a bifurcation in the laminar regime [13]. The random switch from one to another, called bistability and generally observed at small yawing angles, might not be activated under certain conditions due to a lack of turbulent energy. Nevertheless, static asymmetric modes are not suppressed in this case. The difference between vertical base pressure gradients of *state T* and *state B*, either during bistability or when the modes are permanently selected, is almost equal to 0.2, which is very close to what is obtained in the case of the top-bottom bistability on the Ahmed body with a base aspect ratio of $H/W = 0.74$ [12].

4.2. Impact on aerodynamic forces

In both cases, the lift is impacted by the modification of the base pressure distribution and bistability generates lift fluctuations between two limit values corresponding to stable configurations at close yawing angles. The lift increase observed for the Mégane is expected because of the formation of a large depression attached to the rear window. With respect to the detached state, the lift coefficient increases from $c_l = 0.186$ to $c_l = 0.229$, that is 23.1%. However, a paradoxical situation is identified on the Kangoo. In spite of the positive sign of the base

pressure gradient when *state T* is selected (which consequently means that the pressure at the bottom of the base is lower than the one at its top), the lift is positive for both wake configurations. It is clarified if the pressure distribution at the base is not seen as the result of the global pressure distribution around the body due to the attached flow but as a consequence of the selected static mode of the wake. Generally speaking, if this apparent paradox is detected for a car, it might then indicate the presence of static asymmetric modes of the wake. In this case, the lift coefficient changes from $c_l = 0.113$ in *state T* to $c_l = 0.144$ in *state B*, that is 27.4%.

The drag coefficients show two different behaviors for both cars. For the Mégane, the large depression created by the flow reattachment leads to a drag increase. The associated coefficient grows from $c_d = 0.362$ in the detached configuration to $c_d = 0.380$ when reattachment occurs, *i.e.* 5%. For the Kangoo, the drag was already characterized as independent of the yawing angle. It is not affected by bistability either as the drag coefficient do not fluctuate a lot around its mean value $c_d = 0.352$.

5. Conclusions and perspectives for future works

The wake flows behind two vehicles whose Reynolds numbers are of the order of 10^6 and with quite different geometries have been characterized. Aerodynamic forces and base pressure were measured and analyzed. The lift and the vertical base pressure gradient were successfully used to detect wake multistability, in particular thanks to brutal changes or sudden increases in their fluctuations. Probability density functions, used to identify preferred solutions for the flow around the vehicles, also allow to obtain conditionally averaged pressure distributions to better characterize each configuration.

Two distinct causes of wake multistability are identified in this work. On the one hand, increasing the yawing angle β would eventually lead to the formation of a strong depression attached to a vehicle whose pressure distribution is almost uniform in the absence of yaw as the Renault Mégane. A critical angle at which the wake fluctuates between the detached and the attached configuration resulting in fluctuations of both the lift and the drag is identified at $\beta = -8.6°$ which corresponds to a lateral wind of about 20 km.h^{-1} while driving at 130 km.h^{-1} and is therefore very likely to happen in real driving conditions.

On the other hand, another kind of wake bistability is also identified for a vehicle whose pressure distribution was characterized by a vertical pressure gradient in the aligned configuration. The Kangoo is found to have a bistable wake at $\beta = 4.0°$ which corresponds to a lateral wind of about 9 km.h^{-1} while driving at 130 km.h^{-1}. Wake bistability has a big impact on the lift but the drag is surprisingly yaw independent. Interestingly, the selection of one static asymmetric mode is possible independently of the yawing angle which proves that such modes govern the wake.

This paper highlights the importance of design optimization when massive flow reattachment might occur. In particular, the influence of lateral wind has to be taken into account as it is almost always present in real driving conditions and has large consequences on both the drag of the car, thus reducing its fuel efficiency, but also on the lift ergo modifying its stability. The 5% drag increase in such case is large with respect to the targeted benefits of optimization. As regards bistability created by static asymmetric mode, the two mirror configuration suggest that a symmetric and highly unstable mode might be selected. This opens a wide range for passive as well as active control. A 9% drag reduction was recently achieved by forcing the wake to remain in this unstable state [23].

Acknowledgments

The authors wish to thank the CNRT R2A for the funding and the GIE-S2A for the technical support during the tests, as well as Renault SA for the vehicles and technical information.

References

References

[1] H. Schlichting, K. Gersten, Boundary layer theory, Springer Verlag, 2000.

[2] P. Bearman, On vortex shedding from a circular cylinder in the critical Reynolds number regime, Journal of Fluid Mechanics 37 (03) (1969) 577–585.

[3] E. Achenbach, E. Heinecke, On vortex shedding from smooth and rough cylinders in the range of Reynolds numbers 6 10^3 to 5 10^6, Journal of Fluid Mechanics 109 (1981) 239–251.

[4] G. Schewe, On the force fluctuations acting on a circular cylinder in crossflow from subcritical up to transcritical Reynolds numbers, Journal of Fluid Mechanics 133 (1983) 265–285.

[5] G. Schewe, Sensitivity of transition phenomena to small perturbations in flow round a circular cylinder, Journal of Fluid Mechanics 172 (1986) 33–46.
[6] C. Farell, J. Blessmann, On critical flow around smooth circular cylinders, Journal of Fluid Mechanics 136 (1983) 375–391.
[7] J. J. Miau, H. W. Tsai, Y. J. Lin, J. K. Tu, C. H. Fang, M. C. Chen, Experiment on smooth, circular cylinders in cross-flow in the critical Reynolds number regime, Experiments in Fluids 51 (4) (2011) 949–967.
[8] Y.-J. Lin, J.-J. Miau, J.-K. Tu, H.-W. Tsai, Nonstationary, three-dimensional aspects of flow around circular cylinder at critical Reynolds numbers, AIAA Journal 49 (9) (2011) 1857–1870.
[9] O. Cadot, A. Desai, S. Mittal, S. Saxena, B. Chandra, Statistics and dynamics of the boundary layer reattachments during the drag crisis transitions of a circular cylinder, Physics of Fluids 27 (1) (2015) 014101.
[10] M. Grandemange, M. Gohlke, O. Cadot, Reflectional symmetry breaking of the separated flow over three-dimensional bluff bodies, Physical Review E 86 (2012) 035302.
[11] M. Grandemange, M. Gohlke, O. Cadot, Turbulent wake past a three-dimensional blunt body. Part 1. Global modes and bi-stability., Journal of Fluid Mechanics 722 (2013) 51–84.
[12] M. Grandemange, M. Gohlke, O. Cadot, Bi-stability in the turbulent wake past parallelepiped bodies with various aspect ratios and wall effects, Physics of Fluids 25 (2013) 95–103.
[13] O. Cadot, A. Evrard, L. Pastur, Imperfect supercritical bifurcation in a three-dimensional turbulent wake, Physical Review E 91 (6).
[14] M. Grandemange, O. Cadot, A. Courbois, V. Herbert, D. Ricot, T. Ruiz, R. Vigneron, A study of wake effects on the drag of the Ahmed squareback model at the industrial scale, Journal of Wind Engineering and Industrial Aerodynamics 145 (2015) 282–291.
[15] R. Volpe, P. Devinant, A. Kourta, Experimental characterization of the unsteady natural wake of the full-scale square back Ahmed body: flow bi-stability and spectral analysis, Experiments in Fluids 56 (5).
[16] A. Perry, M. Almond, M. Passmore, R. Littlewood, The study of a bi-stable wake region of a generic squareback vehicle using tomographic PIV, SAE Int. J. Passeng. Cars - Mech. Syst 9 (2016) 2.
[17] O. Cadot, A. Courbois, D. Ricot, T. Ruiz, F. Harambat, V. Herbert, R. Vigneron, J. Délery, Characterisations of force and pressure fluctuations of real vehicles, Int. J. Engineering Systems Modelling and Simulation 8 (2) (2016) 99–105.
[18] W. Meile, T. Ladinek, G. Brenn, A. Reppenhagen, A. Fuchs, Non-symmetric bi-stable flow around the Ahmed body, International Journal of Heat and Fluid Flow 57 (2016) 34–47.
[19] S. Ahmed, G. Ramm, G. Faitin, Some salient features of the time-averaged ground vehicle wake, SAE Technical Paper Series 840300.
[20] P. Waudby-Smith, T. Bender, R. Vigneron, The GIE S2A full-scale aeroacoustic wind tunnel, SAE Technical Paper Series 2004-01-0808.
[21] A. Roshko, Perspectives on bluff body aerodynamics, Journal of Wind Engineering and Industrial Aerodynamics 49 (1-3) (1993) 79–100.
[22] W.-H. Hucho, The Aerodynamic Drag of Cars Current Understanding, Unresolved Problems, and Future Prospects, in: Aerodynamic drag mechanisms of bluff bodies and road vehicles, Springer, 1978, pp. 7–44.
[23] A. Evrard, O. Cadot, V. Herbert, D. Ricot, R. Vigneron, J. Délery, Fluid force and symmetry breaking modes of a 3d bluff body with a base cavity, Journal of Fluids and Structures 61 (2016) 99–114.